

Acoustic NLOS Imaging with Cross-Modal Knowledge Distillation

Ui-Hyeon Shin¹, Seungwoo Jang¹ and Kwangsu Kim²

¹Department of Artificial Intelligence, Sungkyunkwan University, Korea

²College of Computing and Informatics, Sungkyunkwan University, Korea

{shineh96, sewo, kim.kwangsu}@skku.edu

Abstract

Acoustic non-line-of-sight (NLOS) imaging aims to reconstruct hidden scenes by analyzing reflections of acoustic waves. Despite recent developments in the field, existing methods still have limitations such as sensitivity to noise in a physical model and difficulty in reconstructing unseen objects in a deep learning model. To address these limitations, we propose a novel cross-modal knowledge distillation (CMKD) approach for acoustic NLOS imaging. Our method transfers knowledge from a well-trained image network to an audio network, effectively combining the strengths of both modalities. As a result, it is robust to noise and superior in reconstructing unseen objects. Additionally, we evaluate real-world datasets and demonstrate that the proposed method outperforms state-of-the-art methods in acoustic NLOS imaging. The experimental results indicate that CMKD is an effective solution for addressing the limitations of current acoustic NLOS imaging methods.

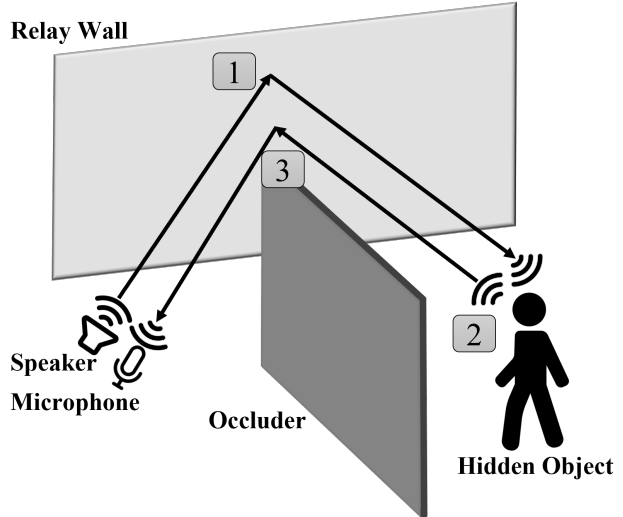


Figure 1: Typical acoustic NLOS setup. The speaker directs acoustic signals toward the hidden space and the microphone measures the three-bounce signals reflected off the hidden objects.

Recently, NLOS imaging methods that utilize acoustic characteristics have been proposed. [Lindell *et al.*, 2019a] proposed a physical model for analyzing acoustic time-of-flight, inspired by seismic imaging. However, NLOS systems typically measure three-bounce reflected signals, as shown in Fig. 1. These signals have low signal intensity, a long travel distance, and high levels of environmental noise. Furthermore, the measurements may be affected by ambient noise, interference, or multipath effects, which can degrade the accuracy and reliability of the time-of-flight estimates. As a result, this approach has only been verified with data collected in a space that is isolated with acoustic foam panels and does not reflect acoustic signals other than those of the relay wall.

To address the limitations of the physical model, [Jang *et al.*, 2022] proposed an end-to-end deep learning model that reconstructs the depth map by extracting the features of hidden scenes from the relative intensity and the arrival time delay of the reflected signal. The model utilizes an encoder with a hierarchical structure to extract acoustic signals from multi-channel audio and the reconstruct hidden scenes in a space where no soundproofing system has been implemented. How-

1 Introduction

Non-line-of-sight (NLOS) imaging [Kirmani *et al.*, 2009] is a method for reconstructing objects or scenes that are hidden from the line-of-sight of an observer. Conventional NLOS imaging methods [Velten *et al.*, 2012; Heide *et al.*, 2014; O’Toole *et al.*, 2018] primarily utilize optical systems in order to infer the properties of hidden scenes. These are achieved by analyzing indirect measurements, such as reflections of optic waves. However, acoustic signals can also be used for NLOS imaging, providing an alternative approach to the analysis of optical signals. Acoustic signals are immune to interference or noise from external sources, such as light or radio frequency radiation. Furthermore, the audible frequency signal exhibits robustness to noise within a specific frequency band, owing to its wide frequency range of 20 Hz to 20 kHz. This makes acoustic NLOS systems more robust and reliable in noise environments, or in situations where the reflections of the optical waves may be distorted or attenuated. In contrast, optical NLOS systems may be affected by noise, which can reduce the quality of the reconstructed image.

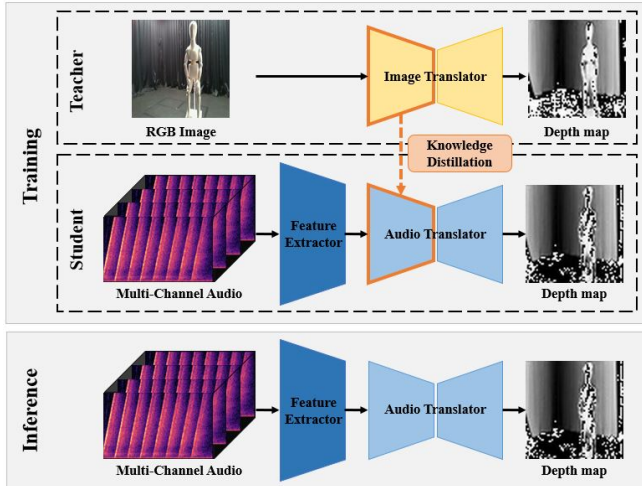


Figure 2: Cross-modal knowledge distillation model transfers knowledge from a well-trained image teacher to an audio student. During inference, the model reconstructs the hidden scene using only audio as input.

ever, the model is limited in its ability to reconstruct unseen objects that are out of distribution with respect to the trained objects.

In general, knowledge distillation [Hinton *et al.*, 2015] has been shown to improve the generalization performance of a target student model by transferring the knowledge of a verified teacher model [Stanton *et al.*, 2021]. Additionally, several studies [Aytar *et al.*, 2016; Albanie *et al.*, 2018; Gan *et al.*, 2019; Valverde *et al.*, 2021] have demonstrated that knowledge distillation between different modalities, such as from image to audio, can further enhance the performance of the target model. Based on these findings, we design a model that is optimized for acoustic NLOS imaging that is intended to be robust to noise and capable of reconstructing unseen objects. To achieve this, we propose a cross-modal knowledge distillation (CMKD) approach that transfer the knowledge of a well-trained image network to an audio network.

The utilization of CMKD allows the strengths of each modality to be used optimally. Image data faithfully represent visual details and spatial information, whereas audio effectively capture dynamic information and potentially useful temporal information. By combining these strengths, the model could achieve better performance than by using either modality alone [Zhao *et al.*, 2018; Gao *et al.*, 2020]. Furthermore, this method enables the model to better generalize to unseen objects and makes the target network robust to noise [Sarfraz *et al.*, 2021].

The CMKD framework consists of an image teacher network and an audio student network shown in Fig. 2. The image teacher network is initially trained to perform the transformation of an RGB image into a depth map. Subsequently, the audio student network is trained to convert multi-channel audio to a depth map, and to leverage the distilled knowledge from the frozen image teacher network. During inference, the audio student network is able to reconstruct the depth map of

a hidden scene using only reflected acoustic signals as input, without any additional image information.

To facilitate this task, we collect a large dataset of 3,600 corresponding frames that consist of RGB images, depth maps, and multi-channel audio. We also construct an acoustic system with eight speaker and microphone arrays and collect 64 channels of reflected signals by transmitting and receiving audible signals (20 Hz to 20 kHz) in a space where no soundproofing system has been implemented. We use this self-collected experimental data to confirm the robustness of our model to noise generated in real-world scenarios.

We compare the performance of our approach with state-of-the-art methods using acquired data. We demonstrate superior performance in reconstructing both trained and unseen objects. We also present detailed ablation studies to highlight the significance of the proposed techniques. Our code, model, and data are available at <https://github.com/shineh96/Acoustic-NLOS-CMKD>. The main contributions of this work are as follows:

- To the best of our knowledge, this is the first instance where CMKD has been applied to NLOS imaging in general, not just in the acoustic domain.
- We collect a new acoustic NLOS dataset and make it available to the public. We hope that this dataset will contribute to the advancement of research in the field of acoustic NLOS.
- Our model demonstrates robustness to real-world noise and enhances the generalization performance on unseen objects, and it outperforms current state-of-the-art models.

2 Related Work

2.1 NLOS Imaging

NLOS imaging has numerous potential applications, including autonomous driving, medical imaging, and rescue operations [Maeda *et al.*, 2019]. A variety of hardware systems, such as pulse lasers and high-resolution detectors [Velten *et al.*, 2012; Liu *et al.*, 2020; Wu *et al.*, 2021], time-of-flight cameras [Heide *et al.*, 2014; Kadambi *et al.*, 2016], conventional cameras [Chen *et al.*, 2019; Henley *et al.*, 2020], LiDAR systems [Zhu and Cai, 2022], and speaker-microphone arrays [Lindell *et al.*, 2019a; Jang *et al.*, 2022], have been used for NLOS imaging. Additionally, several methods have been proposed, including time-of-flight-based models [Velten *et al.*, 2012; Heide *et al.*, 2014] that use directivity and wave-based models [Lindell *et al.*, 2019b] that use diffraction. However, NLOS imaging is an ill-posed problem with a low signal-to-noise ratio, due to the fact that it relies on the analysis of three-bounce reflected signals [Geng *et al.*, 2021]. This can make it challenging to achieve high-quality reconstruction of the hidden scene.

To address this problem, several NLOS imaging methods that use deep learning [Chen *et al.*, 2019; Grau Chopite *et al.*, 2020; Shen *et al.*, 2021] have been proposed. These methods have been successful in reconstructing hidden scenes by distinguishing noise and extracting meaningful features. However, it is important to note that the performance of deep

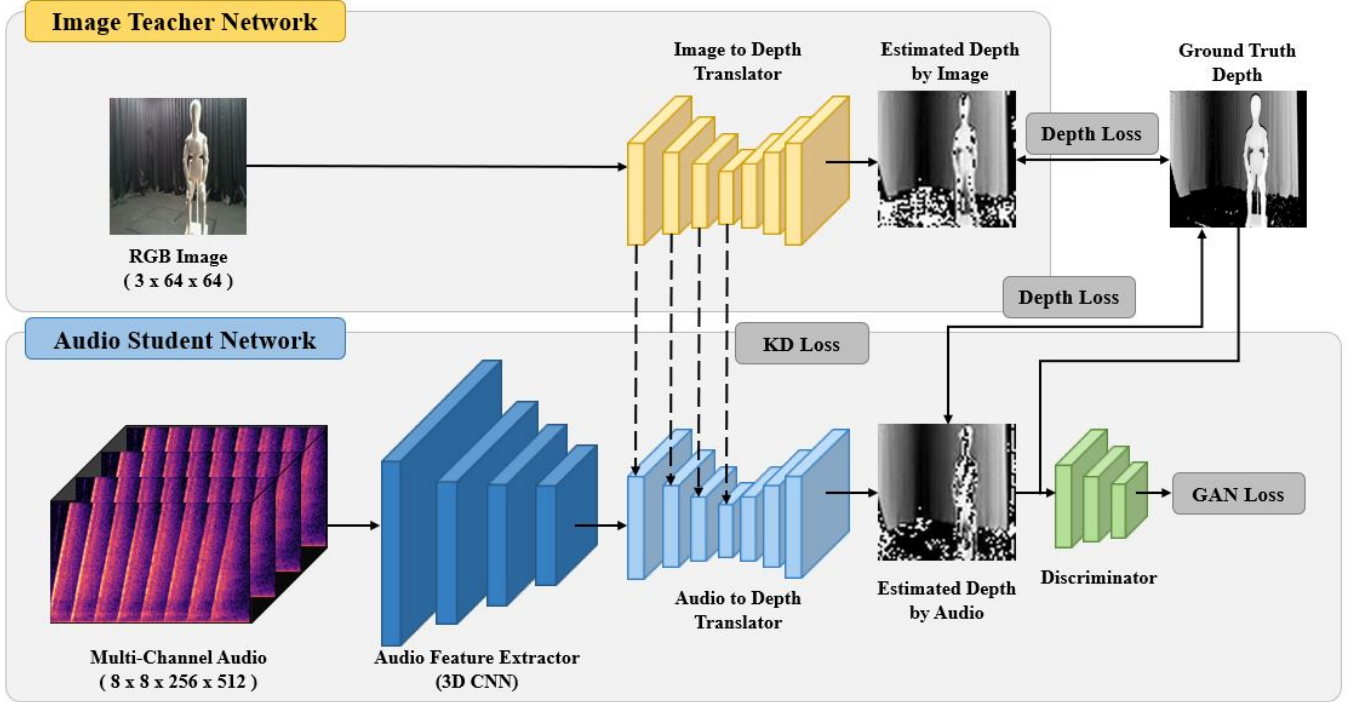


Figure 3: Overview of acoustic NLOS imaging using a cross-modal knowledge distillation (CMKD) framework. This framework consists of two main components: an image teacher network and an audio student network.

learning models heavily relies on the quantity and quality of the dataset. In particular, it is difficult to construct large datasets using optical equipment for NLOS imaging. This is primarily due to the directivity of light, which results in a long collection time of 1 - 5 minutes per sample using point-by-point scanning. As a result, most deep learning methods rely on synthesized data for training and evaluation, as it can be impractical to collect large amounts of real-world data. In contrast, we reduce the collection time to 25 seconds by using an acoustic system that can scan hidden spaces at once. This enables the collection of a larger and higher-quality dataset, which is crucial for the performance of deep learning models.

3 Methodology

In this section, we provide a detailed description of the overall framework and the role of each component, as well as the knowledge transfer method between the two modalities and the loss function used for network learning.

The goal of this framework is to reconstruct the depth map for the hidden scene by transferring knowledge from an image modality to an audio modality. To achieve this, we use an RGB image as the teacher modality and multi-channel audio as the student modality. We employ a two-phase approach, where the first phase involves training the teacher network to transform an RGB image to a depth map. Then, in the second phase, the weights of the well-trained teacher network are frozen, and a student network is trained to convert multi-channel audio to a depth map using the distilled knowledge supplied by the teacher network.

3.1 Cross-Modal Knowledge Distillation

In our approach, we use this method to transfer the knowledge of a well-trained RGB image to depth network to the audio to depth network, with the goal of improving the reconstruction performance of the audio network. During training, we learn both the image and audio modalities, but during inference, we only use the audio modality. This approach allows us to effectively transfer the knowledge of the image network to the audio network, resulting in improved performance.

To facilitate CMKD, the translators of the two sub-networks are designed to have the same structure. We compare three cases of transferring knowledge from the image teacher network to the audio student network: encoder knowledge, decoder knowledge, and whole network knowledge. The results show that transferring only the knowledge of the encoders leads to the greatest improvement in the performance of the audio network. The detailed results of this experiment can be found in the supplementary material. Based on these findings, we present optimal conditions for CMKD in acoustic NLOS imaging.

3.2 Network Architecture

The network architecture consists of two main components: an image teacher network and an audio student network.

Image Teacher Network

The image teacher network is a translator that converts RGB images into depth maps. We adopt a U-Net [Ronneberger *et al.*, 2015] structure auto-encoder as the translator network. The U-Net has been shown to perform well on the task of

210 monocular depth estimation [Alhashim and Wonka, 2018],
211 which involves converting each pixel of an RGB image to a
212 depth value.

213 The U-Net translator consists of an encoder that extracts
214 features from an RGB image and a decoder that reconstructs
215 the latent vector as a depth map. The encoder and decoder
216 are symmetrical, and the high-dimensional information from
217 the encoder is transmitted to the decoder through skip connec-
218 tions. This image network learns the knowledge that is
219 required to convert RGB images to depth maps.

220 **Audio Student Network**

221 The audio student network consists of three main compo-
222 nents: a feature extractor optimized for multi-channel audio
223 input, a translator that converts the extracted audio features to
224 a depth map, and a discriminator that distinguishes whether
225 the estimated depth map is real or fake. The feature extract-
226 tor is responsible for extracting meaningful features from the
227 multi-channel audio input, these features are then passed to
228 the translator. The translator uses these features to reconstruct
229 the depth map of the hidden space. The discriminator is used
230 to evaluate the quality of the reconstructed depth map and
231 distinguish between real and fake examples.

232 The audio network feature extractor is designed specifi-
233 cally to manage multi-channel audio data that are acquired
234 from various locations. The audio data are acquired using an
235 8×8 grid of vertically arranged speaker-microphone pairs that
236 move horizontally. To extract features from the 1D time series
237 data, we apply a short-time Fourier transform to convert the
238 data into a 2D spectrogram having dimensions of 256×512 .
239 The resulting 4D audio data ($8 \times 8 \times 256 \times 512$) are input into
240 the network and passed through eight encoding blocks that
241 extract features using 3D convolution operations [Tran *et al.*,
242 2015] and two fully connected layers that transform the lat-
243 ent vector to the input form for the next network. Each en-
244 coding block consists of a 3D convolutional layer, a 3D batch
245 normalization layer, and a ReLU activation function. This
246 network effectively extracts features from the 4D audio data
247 while preserving the location information.

248 The translator in the audio network has the same structure
249 as the image network, which allows for the transfer of knowl-
250 edge from the image network to the audio network. This
251 structure, which is based on the RGB image to depth map
252 translator, helps to improve the reconstruction performance
253 of the audio network. In addition, the student translator is ini-
254 tialized with the pre-trained weights of the teacher network in
255 order to accelerate learning and further improve reconstruc-
256 tion performance.

257 We adopt the discriminator structure from Pix2Pix [Isola
258 *et al.*, 2017]. The discriminator serves the purpose of distin-
259 guishing whether the estimated depth map is real or fake. The
260 discriminator aligns the distribution of the prediction depth
261 map with the ground truth depth map.

262 **3.3 Objective**

263 **Image Teacher Network**

The image network is trained using only the depth Loss,
which is the pointwise L1 error between the estimated depth
map and the actual depth map. The objective of the image

network is as follows:

$$G_t^* = \min_{G_t} \mathcal{L}_{Depth}(G_t), \quad (1)$$

264 where, G_t is a teacher network generator that translates the
265 RGB image to the depth map.

266 **Audio Student Network**

267 The audio network employs knowledge distillation to en-
268 hance the performance of the conditional adversarial network
269 for audio to depth map translation. Therefore, it is trained
270 by integrating the loss for the conditional adversarial net-
271 work with the loss for the knowledge distillation. We utilize
272 a conditional adversarial network loss based on the Batvi-
273 sion [Christensen *et al.*, 2020] and we measure the depth
274 map reconstruction error using the pointwise L1 error. The
275 GAN loss is determined by the least-squares loss [Mao *et al.*,
276 2017]. In order to align the audio network with the image
277 network, the distance between the feature map distributions
278 of each translator encoding block should be minimized. Our
279 network is designed to minimize this distance as measured by
280 the Kullback-Leibler divergence (KL divergence) [Hinton *et*
281 *al.*, 2015]. The objective of the audio network is as follows:

$$G_s^* = \min_{G_s} \max_{D_s} \frac{1}{2} \mathcal{L}_{GAN}(D_s) + \mathcal{L}_{GAN}(G_s) + \\ \alpha \mathcal{L}_{Depth}(G_s) + \beta \mathcal{L}_{KD}(G_s), \quad (2)$$

282 where, G_s is the generator of the student network, and D_s is
283 the discriminator of the student network. α and β are balanc-
284 ing weights. We set α to 100 and β to 0.01.

285 **4 Experiment**

286 In this section, we describe the data acquisition system for
287 acoustic NLOS imaging and the details of the experimental
288 setup using the acquired dataset. We then evaluate the per-
289 formance of CMKD approach for NLOS imaging and com-
290 pare it with state-of-the-art methods for both LOS and NLOS
291 acoustic imaging. We demonstrate the superiority for unseen
292 object reconstruction and present detailed ablation studies to
293 highlight the contributions of techniques in our method.

294 **4.1 Data**

295 The data used in the experiments and evaluations were self-
296 collected and are representative of real-world scenarios. Us-
297 ing self-acquired data, rather than synthetic or simulated data,
298 enhances the external validity of the results and makes it more
299 likely that the results can be generalized to real-world scenar-
300 os. In this subsection, we describe the experimental setup,
301 data acquisition equipment, and processes used in this study
302 on acoustic NLOS imaging.

303 We conduct the experiments in a space without sound-
304 proofing. The experimental setup includes an occluder that
305 separates the scanning space from the hidden space shown
306 on the left side of Fig. 4. The right side of Fig. 4 illus-
307 trates the configuration of the acoustic system. The system
308 consists of eight sets of speakers and microphones, an audio
309 interface, and a power amplifier. A translation stage is po-
310 sitioned at a 45-degree angle to the relay wall, to move the
311 speaker-microphone array horizontally.

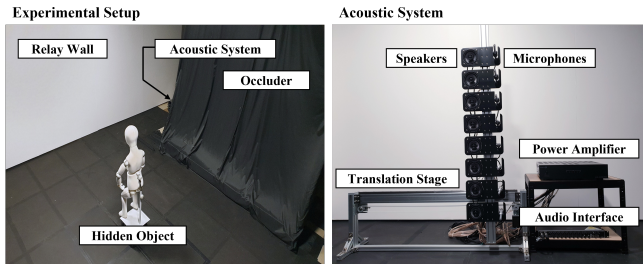


Figure 4: Experimental setup for NLOS imaging (left) and the configuration of the acoustic system for data acquisition (right).

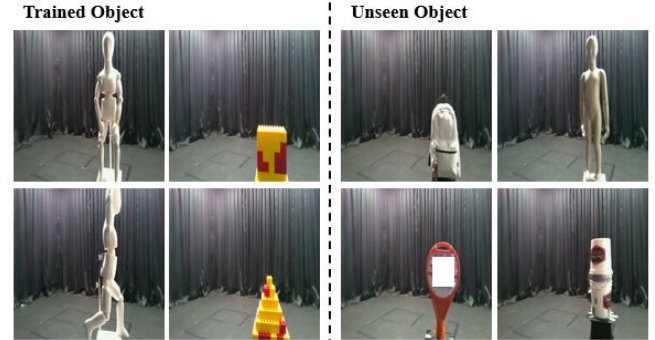


Figure 5: Target objects used for data acquisition are divided into training objects and unseen objects. Training objects include mannequins and plastic models, while unseen objects include bags, plastic signs and various types of mannequins that are different from the training mannequin.

target object. To address this issue, we evaluate the depth map reconstruction error for the object region only, excluding the background.

4.3 Baselines

We compare the performance of CMKD method with both LOS and NLOS acoustic imaging approaches. A physical model [Lindell *et al.*, 2019a] reconstructs a hidden scene based on the analysis of acoustic time-of-flight. A Bativision [Christensen *et al.*, 2020] is a state-of-the-art deep learning method for LOS acoustic imaging, which consists of an audio feature extractor, an auto-encoder, and a discriminator. A hierarchical audio encoder (HAE) [Jang *et al.*, 2022] is a deep learning method for NLOS acoustic imaging that extracts audio features through the HAE that considers the location characteristics of multi-channel audio.

4.4 Experimental Results

We conduct experiments on both trained and unseen objects from the acquired dataset. We compare the performance of our method with several state-of-the-art acoustic imaging baseline methods using both quantitative and qualitative evaluation.

Quantitative Evaluation

In order to perform a quantitative evaluation, we evaluate the reconstruction error for only the object region to use depth estimation metrics. The physical model has limited capability for high resolution depth map reconstruction, which makes it difficult to directly compare it with other models. Therefore, we compare quantitative evaluations of proposed model with those of other baseline models

In Tab. 1, CMKD shows the best performance in terms of quantitative evaluation on both trained and unseen objects. In particular, the threshold accuracy (δ_i), which represents accuracy within certain tolerances, of our method shows a 10 - 20% improvement over that of other methods. Although the RMSE of our model is slightly higher than that of other models, the difference is small, ranging from 1 - 5%. Other methods tend to blur areas where objects are expected to be, as

297 In the acoustic data acquisition process, we employ a se-
298 quential emission method. This method emits linear chirp
299 signals by eight speakers in the audible frequency range (20
300 Hz to 20 kHz), each lasting for 0.1 seconds. To acquire the
301 acoustical data, eight microphones were placed at intervals
302 of 10 cm, with the speakers emitting linear chirp signals se-
303 quentially for a total of 0.8 seconds. The reflected signal is
304 recorded simultaneously on all eight microphones for a du-
305 ration of 0.9 seconds at a sampling rate of 48 kHz, where
306 the time required for the last emitted signal to be reflected
307 back is 0.1 seconds. The acoustic data were then collected at
308 eight points, with the speaker-microphone array moving hor-
3091 zizontally at intervals of 5 cm. Along with the acoustic data,
310 we also acquired RGB images and depth maps as the ground
311 truth for the hidden scene.

312 We acquired data using 30 different kinds of objects, in-
313 cluding mannequins, plastic models, and other objects. The
314 mannequins were posed differently for each class, and the
315 plastic models were made to have various shapes such as hex-
316 ahedrons and pyramids. Other objects included items such as
317 paper boxes, backpacks, and plastic signs. Fig. 5 shows some
318 examples of the target objects that were used for data acqui-
319 sition. Each object is acquired 120 times at different angles
320 and positions, resulting in a total of 3,600 time-synchronized
321 RGB images, as well as depth maps and multi-channel audio.

4.2 Experimental Settings

Data Split

324 During the training process, we utilize only the mannequin
325 and plastic model data. The data for the training objects are
326 divided into 1920 samples for training, 240 samples for val-
327 idation, and 240 samples for testing. The remaining objects,
328 which are not used for training, are utilized to evaluate the
329 model performance on unseen object reconstruction with a
330 total of 1200 data samples

Evaluation Metric

331 To evaluate the performance of methods for the depth map
332 reconstruction of hidden scenes, we utilize metrics commonly
333 used in depth estimation tasks [Alhashim and Wonka, 2018].

334 It is important to note that all data were acquired with the
335 same background, and the size of the object region is only
336 about 10% of the background region on average. Therefore,
337 if the entire depth map is evaluated, a network that performs
338 well on estimating the depth of the background may appear
339 superior to a network that accurately predicts the depth of the
340

341
342
343

344

345
346
347
348
349
350
351
352
353
354
355

356

357
358
359
360
361

362

363
364
365
366
367
368
369
370
371
372
373
374
375
376
377

Trained Objects					
Approach	Rel(\downarrow)	RMSE(\downarrow)	$\delta_1(\uparrow)$	$\delta_2(\uparrow)$	$\delta_3(\uparrow)$
Batvision	5.311	0.288	44.3	56.5	64.2
HAE	3.539	0.288	49.4	60.4	67.8
CMKD (Ours)	2.994	0.293	57.2	65.9	71.7

Table 1: Results of the quantitative evaluation. The left side represents the results for trained objects, and the right side represents the results for unseen objects. Rel is the relative error, and RMSE is the root mean square error. δ_i is the percentage of pixels for which the depth estimates are within a certain range of the true depths. “ \uparrow ” means that higher is better and “ \downarrow ” means that lower is better.

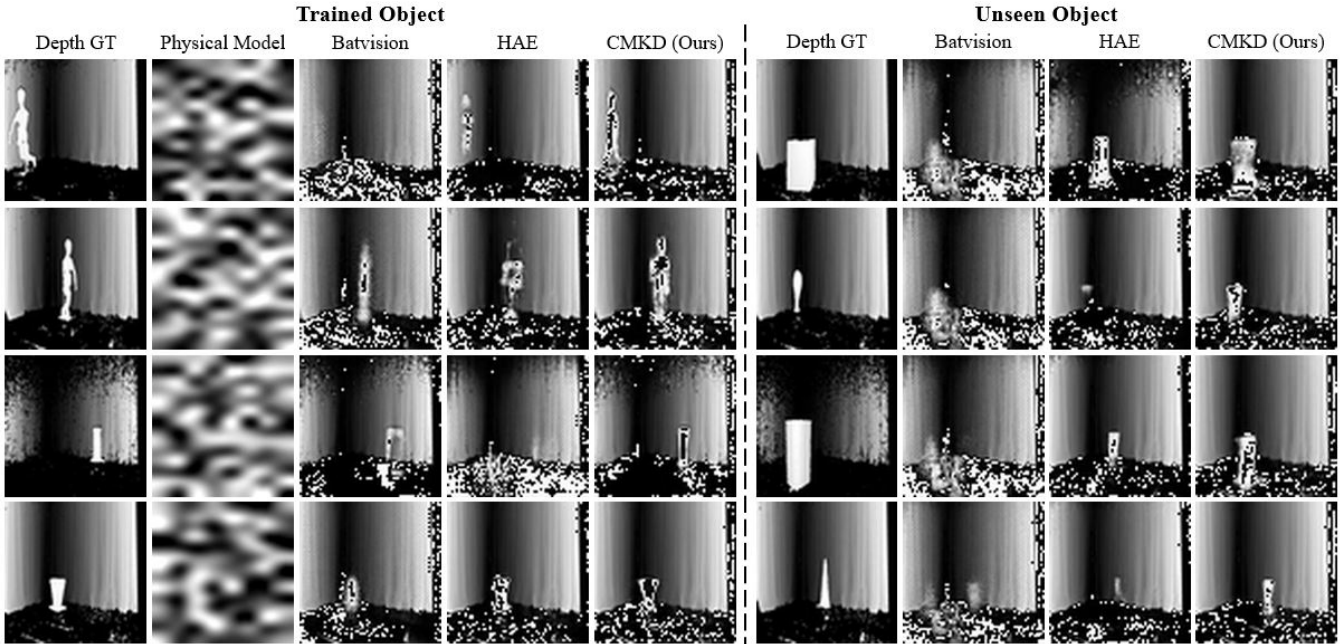


Figure 6: Visualized results of the qualitative evaluation. The left side shows the results for trained objects, and the right side shows the results for unseen objects. CMKD model is able to clearly reconstruct the shape of both trained and unseen objects. In contrast, the baseline models either produce blurry reconstructions or fail to detect the unseen objects.

they focus on reducing pixel-wise loss. This is further demonstrated in the qualitative results.

Qualitative Evaluation

In this subsection, we qualitatively evaluate the performance of CMKD framework for acoustic NLOS imaging. Fig. 6 shows the visualized results for depth map reconstruction for trained and unseen objects, respectively.

Our experiments are conducted in a non-soundproofed environment with ambient noise and overlapping reflections, which can be challenging for the physical model. However, deep learning models, including our model, accurately reconstruct the background due to their ability to learn from data with the same background.

In the case of trained objects, both Batvision and HAE approximate the location of hidden objects and reconstruct their shapes. However, these baseline models sometimes fail to accurately detect object locations and the shapes of their reconstructions are not always clear. In contrast, CMKD model accurately estimates both the shape and distance of the hid-

den object, and it accurately detects the area where the object is located.

Additionally, we evaluate the generalization performance of these models through experiments on unseen objects. While most deep learning-based methods detect the areas where hidden objects are located, Batvision struggles to accurately estimate object shapes and tends to reconstruct blurry depth maps. HAE reconstructs box-shaped objects relatively well, but performs poorly on untrained objects of other shapes. In contrast, CMKD model accurately reconstructs both the position and shape of the object thanks to the transfer of knowledge from the image teacher network, which is not utilized by the other methods.

Other deep learning baselines rely on the pixel-wise loss. However, in some cases, using the pixel-wise loss function may lead to a blurry reconstruction because the model is unable to capture fine-grained details or sharp edges in the image. This can occur if the model does not have enough capacity or if the training data are not representative of the test data. In contrast, our model utilizes knowledge distillation

417 loss, which focuses on predicting the shape of the hidden ob-
 418 ject by transferring knowledge from the image network and
 419 results in more distinct shapes in the reconstructed depth map.

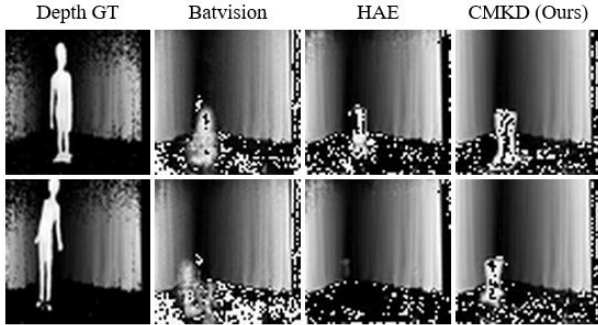


Figure 7: Poor reconstruction results on unseen objects. Deep learning models are limited in their ability to reconstruct objects that differ in material and type from the trained objects. However, our model still shows better reconstruction results than the baseline models.

420 Fig. 7 shows the poor reconstruction results on unseen ob-
 421 jects that differ in material from the trained objects. However,
 422 even in these cases, other models either fail to predict the po-
 423 sition of the object or produce a blurry reconstruction, while
 424 our model still accurately estimates the position of the hidden
 425 object and relatively accurately reconstructs its size. There is
 426 a limitation in acoustic NLOS imaging as the reflected sig-
 427 nals can vary significantly depending on the material or type
 428 of hidden objects. This issue can potentially be addressed by
 429 increasing the diversity of collected objects, as the types of
 430 trained data are limited and tend to have similar shapes, ma-
 431 terials, and sizes. In our future research, we aim to address
 432 this issue by expanding our data acquisition to encompass a
 433 broader range of objects with varying shapes, materials, and
 434 sizes.

435 Ablation study

	Extractor	KD	Rel(\downarrow)	RMSE(\downarrow)	$\delta_1(\uparrow)$	$\delta_2(\uparrow)$	$\delta_3(\uparrow)$
(a)	3D CNN	X	7.888	0.399	31.6	42.0	49.1
(b)	2D CNN	O	8.027	0.397	36.8	46.9	53.7
(c)	HAE		7.479	0.396	36.8	46.8	53.4
(d)	3D CNN		7.094	0.392	40.0	49.9	56.2

Table 2: Results of ablation studies. (a) Performance when knowledge distillation is not applied to the audio network structure. (b), (c) Performances when the audio feature extractor is replaced with a 2D CNN and a hierarchical 2D CNN, respectively. (d) Our method using a 3D CNN feature extractor and knowledge distillation.

436 In Tab. 2, we present the results of ablation studies which
 437 were conducted to evaluate the effectiveness of the techniques
 438 used in CMKD method. The results are presented in the form
 439 of a comparison between different configurations. The com-
 440 parison of configurations (a) and (d) demonstrate the effect
 441 of knowledge distillation, whereas the comparison of config-
 442 urations (b), (c) and (d) demonstrate the performance of each
 443 feature extractor. We can observe that using the 3D CNN

feature extractor and incorporating knowledge distilled from
 444 the image network significantly improves the reconstruction
 445 of hidden objects in acoustic NLOS imaging. These findings
 446 confirm the effectiveness of the techniques and structures im-
 447 plemented in the proposed model.
 448

5 Conclusion

In this paper, we propose a method for improving the per-
 450 formance of acoustic NLOS imaging systems. While pre-
 451 vious approaches to acoustic NLOS imaging have encoun-
 452 tered limitations, such as vulnerability to noise and difficulty
 453 in reconstructing unseen objects, our method uses CMKD
 454 to transfer knowledge from a well-trained image network
 455 to an audio network. This enables the resulting model to
 456 be robust to noise and to enhance the generalization perfor-
 457 mance on unseen objects. Our experimental results show
 458 that CMKD method outperforms state-of-the-art methods in
 459 acoustic NLOS imaging and demonstrates superior perfor-
 460 mance in reconstructing unseen objects. Additionally, the re-
 461 sults of the ablation studies demonstrate the suitability of the
 462 techniques and structures implemented in the proposed model
 463 for acoustic NLOS imaging. Overall, we provide a promis-
 464 ing solution for acoustic NLOS imaging, and has potential for
 465 various practical applications in the future.
 466

References

- [Albanie *et al.*, 2018] Samuel Albanie, Arsha Nagrani, Andrea Vedaldi, and Andrew Zisserman. Emotion recognition in speech using cross-modal transfer in the wild. In *Proceedings of the 26th ACM international conference on Multimedia*, pages 292–301, 2018.
- [Alhashim and Wonka, 2018] Ibraheem Alhashim and Peter Wonka. High quality monocular depth estimation via transfer learning. *arXiv preprint arXiv:1812.11941*, 2018.
- [Aytar *et al.*, 2016] Yusuf Aytar, Carl Vondrick, and Antonio Torralba. Soundnet: Learning sound representations from unlabeled video. *Advances in neural information processing systems*, 29, 2016.
- [Chen *et al.*, 2019] Wenzheng Chen, Simon Daneau, Fahim Mannan, and Felix Heide. Steady-state non-line-of-sight imaging. In *Proceedings of the IEEE/CVF Conference on Computer Vision and Pattern Recognition*, pages 6790–6799, 2019.
- [Christensen *et al.*, 2020] Jesper Haahr Christensen, Sascha Hornauer, and X Yu Stella. Batvision: Learning to see 3d spatial layout with two ears. In *2020 IEEE International Conference on Robotics and Automation (ICRA)*, pages 1581–1587. IEEE, 2020.
- [Gan *et al.*, 2019] Chuang Gan, Hang Zhao, Peihao Chen, David Cox, and Antonio Torralba. Self-supervised moving vehicle tracking with stereo sound. In *Proceedings of the IEEE/CVF International Conference on Computer Vision*, pages 7053–7062, 2019.
- [Gao *et al.*, 2020] Ruohan Gao, Changan Chen, Ziad Al-Halah, Carl Schissler, and Kristen Grauman. Visualechoes: Spatial image representation learning through

- 498 echolocation. In *European Conference on Computer Vi-*
499 *sion*, pages 658–676. Springer, 2020.
- 500 [Geng *et al.*, 2021] Ruixu Geng, Yang Hu, Yan Chen, et al.
501 Recent advances on non-line-of-sight imaging: Conven-
502 tional physical models, deep learning, and new scenes.
503 *APSIPA Transactions on Signal and Information Process-
504 ing*, 11(1), 2021.
- 505 [Grau Chopite *et al.*, 2020] Javier Grau Chopite, Matthias B
506 Hullin, Michael Wand, and Julian Iseringhausen. Deep
507 non-line-of-sight reconstruction. In *Proceedings of the
508 IEEE/CVF Conference on Computer Vision and Pattern
509 Recognition*, pages 960–969, 2020.
- 510 [Heide *et al.*, 2014] Felix Heide, Lei Xiao, Wolfgang Hei-
511 drich, and Matthias B Hullin. Diffuse mirrors: 3d recon-
512 struction from diffuse indirect illumination using inex-
513 pensive time-of-flight sensors. In *Proceedings of the IEEE
514 Conference on Computer Vision and Pattern Recognition*,
515 pages 3222–3229, 2014.
- 516 [Henley *et al.*, 2020] Connor Henley, Tomohiro Maeda,
517 Tristan Swedish, and Ramesh Raskar. Imaging behind oc-
518 cluders using two-bounce light. In *European Conference
519 on Computer Vision*, pages 573–588. Springer, 2020.
- 520 [Hinton *et al.*, 2015] Geoffrey Hinton, Oriol Vinyals, Jeff
521 Dean, et al. Distilling the knowledge in a neural network.
522 *arXiv preprint arXiv:1503.02531*, 2015.
- 523 [Isola *et al.*, 2017] Phillip Isola, Jun-Yan Zhu, Tinghui Zhou,
524 and Alexei A Efros. Image-to-image translation with con-
525 ditional adversarial networks. In *Proceedings of the IEEE
526 conference on computer vision and pattern recognition*,
527 pages 1125–1134, 2017.
- 528 [Jang *et al.*, 2022] Seungwoo Jang, Ui-Hyeon Shin, and
529 Kwangsu Kim. Deep non-line-of-sight imaging using
530 echolocation. *Sensors*, 22(21):8477, 2022.
- 531 [Kadambi *et al.*, 2016] Achuta Kadambi, Hang Zhao, Boxin
532 Shi, and Ramesh Raskar. Occluded imaging with time-
533 of-flight sensors. *ACM Transactions on Graphics (ToG)*,
534 35(2):1–12, 2016.
- 535 [Kirmani *et al.*, 2009] Ahmed Kirmani, Tyler Hutchison,
536 James Davis, and Ramesh Raskar. Looking around the
537 corner using transient imaging. In *2009 IEEE 12th Inter-
538 national Conference on Computer Vision*, pages 159–166.
539 IEEE, 2009.
- 540 [Lindell *et al.*, 2019a] David B Lindell, Gordon Wetzstein,
541 and Vladlen Koltun. Acoustic non-line-of-sight imaging.
542 In *Proceedings of the IEEE/CVF Conference on Computer
543 Vision and Pattern Recognition*, pages 6780–6789, 2019.
- 544 [Lindell *et al.*, 2019b] David B Lindell, Gordon Wetzstein,
545 and Matthew O’Toole. Wave-based non-line-of-sight
546 imaging using fast fk migration. *ACM Transactions on
547 Graphics (ToG)*, 38(4):1–13, 2019.
- 548 [Liu *et al.*, 2020] Xiaochun Liu, Sebastian Bauer, and
549 Andreas Velten. Phasor field diffraction based reconstruc-
550 tion for fast non-line-of-sight imaging systems. *Nature com-
551 munications*, 11(1):1–13, 2020.
- 552 [Maeda *et al.*, 2019] Tomohiro Maeda, Guy Satat, Tristan
553 Swedish, Lagnojita Sinha, and Ramesh Raskar. Re-
554 cent advances in imaging around corners. *arXiv preprint
555 arXiv:1910.05613*, 2019.
- 556 [Mao *et al.*, 2017] Xudong Mao, Qing Li, Haoran Xie, Ray-
557 mond YK Lau, Zhen Wang, and Stephen Paul Smolley.
558 Least squares generative adversarial networks. In *Pro-
559 ceedings of the IEEE international conference on computer vi-
560 sion*, pages 2794–2802, 2017.
- 561 [O’Toole *et al.*, 2018] Matthew O’Toole, David B Lindell,
562 and Gordon Wetzstein. Confocal non-line-of-sight
563 imaging based on the light-cone transform. *Nature*,
564 555(7696):338–341, 2018.
- 565 [Ronneberger *et al.*, 2015] Olaf Ronneberger, Philipp Fischer,
566 and Thomas Brox. U-net: Convolutional networks
567 for biomedical image segmentation. In *International
568 Conference on Medical image computing and computer-
569 assisted intervention*, pages 234–241. Springer, 2015.
- 570 [Sarfraz *et al.*, 2021] Fahad Sarfraz, Elahe Arani, and
571 Bahram Zonooz. Knowledge distillation beyond model
572 compression. In *2020 25th International Conference
573 on Pattern Recognition (ICPR)*, pages 6136–6143. IEEE,
574 2021.
- 575 [Shen *et al.*, 2021] Siyuan Shen, Zi Wang, Ping Liu,
576 Zhengqing Pan, Ruiqian Li, Tian Gao, Shiyi Li, and
577 Jingyi Yu. Non-line-of-sight imaging via neural transient
578 fields. *IEEE Transactions on Pattern Analysis and Ma-
579 chine Intelligence*, 43(7):2257–2268, 2021.
- 580 [Stanton *et al.*, 2021] Samuel Stanton, Pavel Izmailov,
581 Polina Kirichenko, Alexander A Alemi, and Andrew G
582 Wilson. Does knowledge distillation really work?
583 *Advances in Neural Information Processing Systems*,
584 34:6906–6919, 2021.
- 585 [Tran *et al.*, 2015] Du Tran, Lubomir Bourdev, Rob Fergus,
586 Lorenzo Torresani, and Manohar Paluri. Learning spa-
587 tiotemporal features with 3d convolutional networks. In
588 *Proceedings of the IEEE international conference on com-
589 puter vision*, pages 4489–4497, 2015.
- 590 [Valverde *et al.*, 2021] Francisco Rivera Valverde, Juana Va-
591 leria Hurtado, and Abhinav Valada. There is more than
592 meets the eye: Self-supervised multi-object detection
593 and tracking with sound by distilling multimodal knowl-
594 edge. In *Proceedings of the IEEE/CVF Conference on
595 Computer Vision and Pattern Recognition*, pages 11612–
596 11621, 2021.
- 597 [Velten *et al.*, 2012] Andreas Velten, Thomas Willwacher,
598 Otkrist Gupta, Ashok Veeraraghavan, Moungi G Bawendi,
599 and Ramesh Raskar. Recovering three-dimensional shape
600 around a corner using ultrafast time-of-flight imaging. *Na-
601 ture communications*, 3(1):1–8, 2012.
- 602 [Wu *et al.*, 2021] Cheng Wu, Jianjiang Liu, Xin Huang,
603 Zheng-Ping Li, Chao Yu, Jun-Tian Ye, Jun Zhang, Qiang
604 Zhang, Xiankang Dou, Vivek K Goyal, et al. Non-line-of-
605 sight imaging over 1.43 km. *Proceedings of the National
606 Academy of Sciences*, 118(10):e2024468118, 2021.

607 [Zhao *et al.*, 2018] Mingmin Zhao, Tianhong Li, Moham-
608 mad Abu Alsheikh, Yonglong Tian, Hang Zhao, Antonio
609 Torralba, and Dina Katabi. Through-wall human pose es-
610 timation using radio signals. In *Proceedings of the IEEE*
611 *Conference on Computer Vision and Pattern Recognition*,
612 pages 7356–7365, 2018.

613 [Zhu and Cai, 2022] Dayu Zhu and Wenshan Cai. Fast non-
614 line-of-sight imaging with two-step deep remapping. *ACS*
615 *Photonics*, 9(6):2046–2055, 2022.